Polym. Bull. (2012) 68:1747–1763
DOI 10.1007/s00289-012-0700-7

ORIGINAL PAPER

Enhanced mechanical and photoluminescence effect of poly(L-lactide) reinforced with functionalized multiwalled carbon nanotubes

Maryam Amirian · Ali Nabipour Chakoli · Jie He Sui · Wei Cai

Received: 23 July 2011 / Revised: 29 November 2011 / Accepted: 2 January 2012 /
Published online: 14 January 2012

Abstract The poly(L-lactide) (PLLA) biocompatible and biodegradable polymer was reinforced with functionalized Multiwalled carbon nanotubes (MWCNTs) to overcome on insufficient mechanical properties of this polymer for high load bearing applications. To fully realize the potential of MWCNTs for this purpose, they have to be homogeneously dispersed in polymer matrix and have efficient load transfer across the MWCNTs/polymer interface. The pristine MWCNTs (pMWCNTs) were functionalized, at first, by Friedel–Crafts acylation, which introduced the aromatic amine groups on the sidewall of MWCNTs (MWCNT–NH_2) without shortening or cutting of pMWCNTs. And then, the PLLA chains covalently grafted from the sidewall of MWCNT–NH_2 by in situ ring-opening polymerization of L-lactide oligomers using stannous octanoate as the initiating system. The Fourier transform infrared spectroscopy and X-ray photoelectron spectroscopy spectra revealed that the PLLA chains grafted form the sidewall of MWCNTs strongly. The surface morphology of pristine and PLLA-grafted MWCNTs (MWCNT-*g*-PLLAs) was characterized by scanning electron microscopy and transmission electron microscopy. The tensile test of prepared composites of PLLA with various concentrations of MWCNT-*g*-PLLAs show a significant increment in tensile strength and elongation at failure of composites with increasing the concentration of MWCNT-*g*-PLLAs in composites. Also, it is found that the MWCNT-*g*-PLLAs increased the photoluminescence effect of PLLA and widened the luminescence region of PLLA.

M. Amirian · J. H. Sui · W. Cai (✉)
School of Materials Science and Engineering, Harbin Institute of Technology,
P. O. Box 405, Harbin 150001, Heilongjiang Province, People's Republic of China
e-mail: weicai@hit.edu.cn

A. Nabipour Chakoli
Materials Research School, NSTRI, P. O. Box 31485-498, Moazen Blv., Rajaeeshahr, Karaj, Iran

Keywords Functionalized carbon nanotubes · Biodegradable polymers · Poly(L-lactide) · Grafting from · Nanocomposites · Photoluminescence

Introduction

In recent years, there have been increasing demands for the use of biodegradable polymers in soft and hard tissue engineering, drug delivery systems, also specifically to minimize polymer waste management caused by non-degradable polymers. Biodegradable polymers are gaining more and more attention because they can be degraded in the environment by the action of naturally occurring microorganisms. Biodegradable polymers can be processed by traditional thermoplastic processing methods, and composting is a sustainable option for their disposal. These materials are not yet broadly used in industry because of their high cost and limited performance for many applications. Reinforcing of biodegradable polymers can also be an approach to overcoming some limitations of single applications of these materials, such as brittleness, low stiffness, and low toughness. Some studies have evaluated the mechanical properties of biodegradable polymer blends. Nowadays, biodegradable polyesters are extensively studied as matrix materials in biocomposites reinforced with various materials for improving their performance. Biocompatible polymers with hydrolyzable chemical bonds are being used to produce safe, non-toxic fluorescent microspheres for material penetration studies. The selection of polymeric materials depends on both biocompatibility and processability, with tailored fluorescent properties depending on specific applications [1–5].

Monitoring and characterization of biological changes in small biomolecules requires fast experimental techniques. Fluorescence spectroscopy has been helpful in accessing the fastest biomolecular processes, such as the folding of small proteins, or polymer dynamics. Also, it is predictable that fluorescence spectroscopy is useful to study the in vivo degradation of biodegradable polymers that have fluorescence effect such as PLLA. The power of fluorescence spectroscopy and microscopy is due to its exquisite selectivity, sensitivity, and multiple observables, that are accessible through fluorescence [6–8].

Carbon nanotubes (CNTs) had been widely attended since they were reported. CNTs exhibited many features such as nanosize, large aspect ratio, low mass density, high flexibility, high mechanical strength, excellent electrical, and thermal properties. The CNTs were classified as single-walled CNTs (SWCNTs) and Multiwalled CNTs (MWCNTs) [9–11]. The CNTs had been applied in many field of science such as polymer and metal composites, biomedical materials, sensors, field emission displays, and nanosize probes. Although there have been some conflicting results about CNTs' safety and biocompatibility in these years, more biomedical applications of CNTs are proposed including biosensors, tissue engineering scaffolds, drug delivery carriers, and other functional devices. The CNTs, which have been used as reinforcing fillers in polymeric biomaterials, will dramatically improve the materials' mechanical strength and simultaneously endow them with electric conductivity that may provide electrical stimulation for tissue engineering

constructs. The use of CNTs in vivo requires appropriate functionalization to reduce toxicity and non-specific binding [12–34].

In this article, we report the synthesis of MWCNT–NH_2s and MWCNT-*g*-PLLAs via grafting from approach and in situ ring-opening polymerizations of L-lactide using stannous octanoate. To investigate the effect of functionalization of MWCNTs, transmission electron microscopy (TEM) and scanning electron microscopy (SEM) has been carried out. The functional groups on the sidewall of MWCNTs were monitored by Fourier transform infrared spectroscopy (FT-IR) and X-ray photoelectron spectroscopy (XPS). To check the mechanical reinforcement of neat PLLA using MWCNT-*g*-PLLAs, we prepared the MWCNT-*g*-PLLAs/PLLA composites. The yield stress, ultimate strength, and elongation at failure of neat PLLA and MWCNT-*g*-PLLAs/PLLA composites have been indicated using tensile test instrument. The fracture morphology of composites were characterized using SEM.

Experimental

Materials

L-Lactide oligomer (Xiaogan Esun New Material Co, China) was used as received. Stannous octanoate ($St(Oct)_2$) (Shanghai chemical reagent company, China) was used as a catalyst. Chloroform, ethanol, methanol, toluene, *p*-amino benzoic acid, poly phosphoric acid, and phosphoric penta oxide (P_2O_5) were purchased from Kermel of China as analytic reagent. Pristine MWCNTs (pMWCNTs) were purchased from the Nanotech Port Company. The diameter of MWCNTs is 5–20 nm, length is 5–15 μm, and special surface area is 40–300 $m^2\ g^{-1}$.

Synthesis of MWCNT–NH_2

Aromatic amines were introduced on the surface of the pMWCNTs by Friedel–Crafts acylation. The *p*-amino benzoic acid, pMWCNTs, and polyphosphoric acid were heated at 120 °C for 3 h. Then, P_2O_5 was added to the mixture, and then the mixture was heated for 12 h. The reacted mixture was cooled and diluted with distilled water, and the precipitates were washed with the ammonium chloride solution. Then, the materials were washed with distilled water and then vacuum-filtered through a 0.22 μm Millipore polycarbonate membrane. The filtered solid was dried in oven at 50 °C overnight. The chemical reaction is schematized in Scheme 1a.

Synthesis of MWCNT-*g*-PLLAs

To synthesis of MWCNT-*g*-PLLAs, L-lactide oligomer were added into a flask with $Sn(Oct)_2$ as initiator and MWCNT–NH_2 as co-initiator. For uniform dispersion of $Sn(Oct)_2$ in flask, we used toluene as solvent. After degassing the flask to remove toluene, the flask was sealed under vacuum and then placed in an oven at 130 °C for 48 h. To remove the ungrafted PLLA chains and monomers, the synthesized

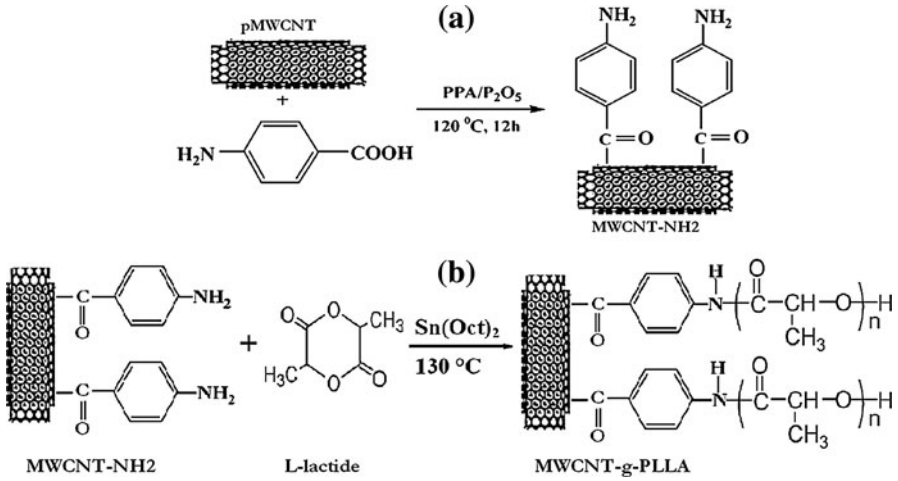

Scheme 1 Scheme of reactions: synthesis of MWCNT–NH_2s (**a**) and MWCNT-*g*-PLLAs (**b**)

material was dissolved in chloroform and vacuum-filtered through a 0.22 μm Millipore polycarbonate membrane four times. Then, the products were dried in an oven at 40 °C for 2 days. The chemical reaction is schematized in Scheme 1b.

Preparation of composites

The MWCNT-*g*-PLLAs, which were dispersed in chloroform with various concentrations, were mixed with the neat PLLA in chloroform to achieve MWCNT-*g*-PLLAs/PLLA composites having 1.0, 2.0, and 3.0 and wt% loading of MWCNT-*g*-PLLAs. The neat PLLA homopolymers were prepared as introduced in our previous works [33]. The mixtures were left in glass molds 3 days at room temperature for chloroform evaporation, then the glass molds contains composite films were dried in an oven at 40 °C for 2 days to complete evaporation of solvent. The film of composites were removed from glass molds and cut for characterization.

Characterization

To check the suspensibility of pMWCNTs, MWCNT–NH_2s, and MWCNT-*g*-PLLAs in water and chloroform, for long time, above materials were dissolved in chloroform and water separately with 0.1 g L^{-1} density and ultrasonicated for 10 min. The samples were put in a free vibration place for a long time to see the solubility or precipitation of dissolved materials in each solution.

The SEM images refer to MWCNTs and the fracture surface of composites were acquired using a Hitachi S-4700 field emission system. The fracture surface of tensile test samples after breaking was sputter coated with a thin layer (ca. 3 nm) of Au prior to SEM imaging. A TEM, HITACH model Mic H-7650 was employed to

investigate the fine nanostructure of synthesized materials. For TEM sample preparation, specimens were dissolved in ethanol and then the solution was dropped on 200-mesh carbon-coated copper grid and dried them at room temperature.

The FT-IR spectra of pristine and functionalized MWCNTs were recorded between 500 and 4,000 cm^{-1} using a Perkin Elmer Spectrum One FT-IR spectrometer. A minimum of 16 scans were averaged with a signal resolution of 4 cm^{-1} within the 500–4,000 cm^{-1} range. The XPS spectra of pristine and functionalized MWCNTs were obtained using a PHI 5700 ESCA spectrometer. Non-monochromatic Al(K_α) photons were used for all the measurements. The atomic composition of the sample surfaces was calculated using the high-resolution peak areas for the main core XPS line of each element in conjunction with the empirical sensitivity factors provided by the instrument manufacturer and the application of a Shirley-type background correction. The binding energy of the C(1*s*) was set at 284.5 eV as the reference for all other peaks.

The X-ray diffraction (XRD) method was employed for studying the crystalline structure by using a Rigaku D/max-rb rotating anode X-ray diffractometer at 50 kV and 40 mA.

The molecular weight and the distribution of the synthesized PLLA was measured by gel permeation chromatography (GPC) using Agilent 1100 series (Agilent, USA). Tetrahydrofuran (THF) was used as the mobile phase at a flow rate of 1.0 mL/min at 30 °C. The RI Mobile Phase detector with two columns Agilent 79911GP-101 and 79911GP-104 (connected in series) are carried out. Calibration was performed with polystyrene (PE) standards to determine the absolute weight-average ($\overline{Mw}$), number-average molecular weight ($\overline{Mn}$), and polydispersity index (P.I.) of prepared neat PLLA. For sample preparation, 40 mg of prepared PLLA is dissolved in 20 mL of THF and magnetic stirred for 5 h to find homogeneous solution.

Tensile properties of PLLA composites were obtained based on ASTM D638 method. The tensile tests were performed using a microcontroller electronic tension meter (model WDW3100) machine at a crosshead speed of 2.5 mm per minute at room temperature. The yield stress, modulus, ultimate strength, and elongation at break of each sample were obtained based on at least three specimens per sample. The photoluminescence (PL) spectra of neat PLLA and composites were taken with a Horiba Jobin–Yvon Fluoromax-4 spectroflurometer system with the 350 nm exciting wavelength at room temperature.

Results and discussions

Suspensibility of MWCNTs

Figure 1 shows the suspensibility of pristine and functionalized MWCNTs in water and chloroform. The suspensions of pristine MWCNTs, MWCNT–NH_2s, and MWCNT-*g*-PLLAs in water and chloroform were checked after 30 min and 2 days. The pMWCNTs and MWCNT-*g*-PLLAs are not suspensible in water. While due to

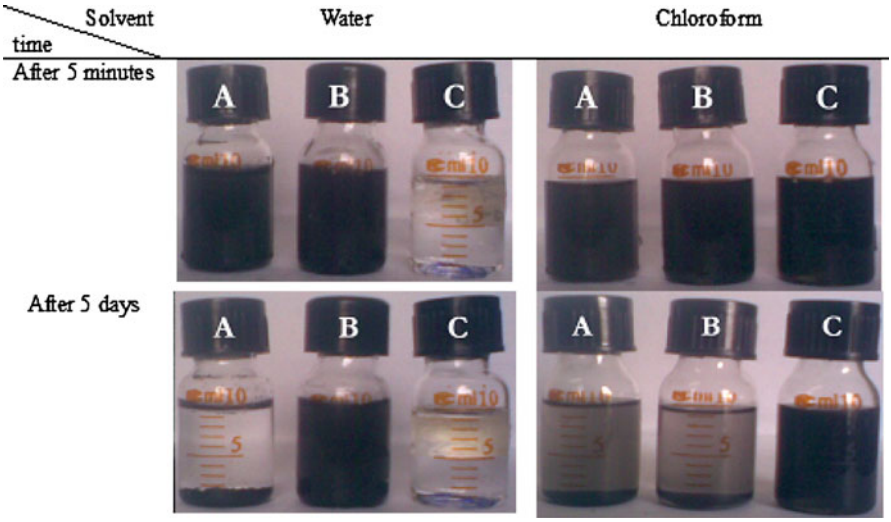

Fig. 1 The suspension stability of pMWCNTs (*a*), MWCNT–NH_2s (*b*), and MWCNT-*g*-PLLAs (*c*) in water and chloroform at room temperature after 30 min and after 5 days

amine groups, MWCNT–NH_2s is suspensible in water. The pMWCNTs is not suspensible in water and the MWCNT–NH_2s is partially suspensible in chloroform and most of them precipitated at bottom. The MWCNT-*g*-PLLAs, due to grafted PLLA chains on the sidewall of MWCNTs are strongly suspensible in chloroform.

Morphology of MWCNTs

Figure 2 gives the surface morphology of pMWCNTs, MWCNT–NH_2s, and MWCNT-*g*-PLLAs. The used pMWCNTs are long and varied in diameter. As can be seen, some of the pMWCNTs were entangeled to each other. The MWCNT–NH_2s, because of purificaion and acylation, has less entengeled points in comparison with pMWCNTs. The MWCNT-*g*-PLACLs have a diameter strongly more than that of MWCNT–NH_2s. The MWCNT-*g*-PLLAs were entangled together at the intersection points. This indicates that the grafting reaction took place over the whole surface of the MWCNTs. The grafted PLLA chains from the MWCNT can entangle with the grafted chains of neighbor MWCNT like brush hair.

Also, the morphology of the pristine and functionalized MWCNTs, were observed using TEM as presented in Fig. 3. The pMWCNTs are long and varied in diameter and some of them are bamboo like. There are many impurities that produced during their manufacture such as metal catalysts and many entangled points that referred to pMWCNTs. As presented in Fig. 3b, c, a core–shell structure of MWCNT–NH_2s at the center can be seen clearly, but the core–shell structure of MWCNT-*g*-PLLA hard to be seen clearly, which indicates that the MWCNT was covalently coated by grafted PLLA chains and the PLLA layer is thick. The MWCNT-*g*-PLLA has two shells. The inside core shell is hard shell that refers to

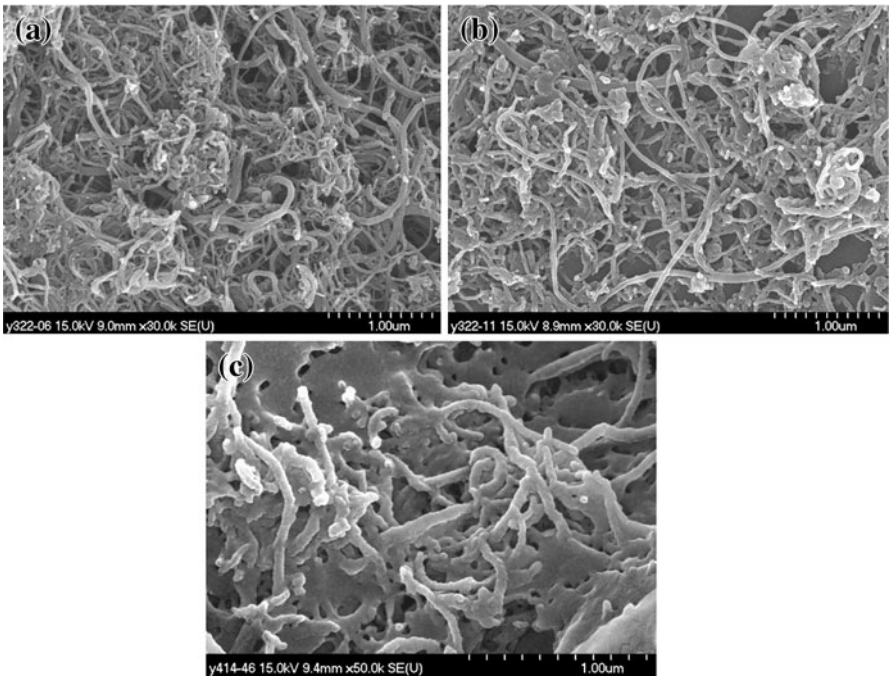

Fig. 2 The SEM micrographs of pMWCNTs (**a**) and MWCNT-*g*-PLACLs (**b**)

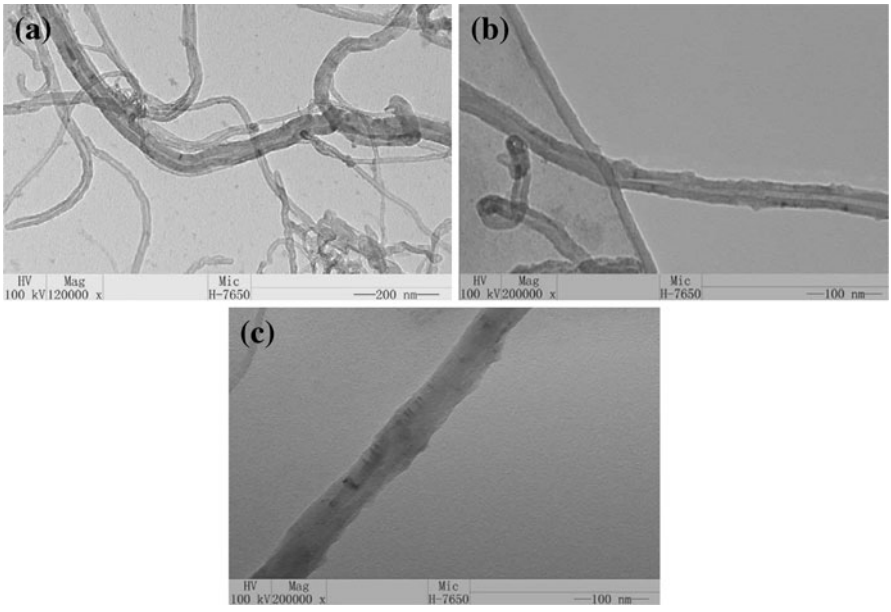

Fig. 3 The TEM micrographs of pristine MWCNT (**a**), MWCNT–NH_2 (**b**), and MWCNT-*g*-PLLA (**c**)

initial MWCNT and the outside shell is soft shell that refers to grafted PLLA polymer chains.

Structural characterization of MWCNTs

Figure 4 shows the FT-IR spectrum of pMWCNTs, MWCNT–NH_2s, and MWCNT-*g*-PLLAs. The pMWCNTs have some weak peaks between 2,980 and 2,840 cm^{-1} corresponds to –CH stretching absorption band. The FT-IR result (–CH stretching) indicates that pMWCNTs contain defects, which may be formed during their manufacture. The FT-IR spectra of MWCNT–NH_2s shows a N–H band at 1,235 cm^{-1}, indicating that functional groups were introduced onto the sidewall of MWCNTs. The NH_2 stretch band appears at 3,420 cm^{-1}. The scissoring in-plane bending mode of the primary amine NH_2 group at 1,645 cm^{-1} is broader than other peaks in this region, such as the carbonyl stretching and aromatic ring modes. A broad band at 758 cm^{-1} is due to the out of plane NH_2 bending mode.

Peaks at 2,930 and 2,859 cm^{-1} in Fig. 4(3) correspond to $–CH_3$ absorption band that belongs to C–H bonds of grafted PLLA chains. The feature at 1,753 cm^{-1} corresponds to the absorption of C=O stretching. It refers to ester groups of grafted PLLA chains. The C–O stretching vibrations of asymmetrical coupled vibration of C–CO–O belong to the PLLA chains. These vibrations are at 1,083 and 1,185 cm^{-1}. The resonances due to $C–CH_3$ stretching, $–CH_3$ rocking mode, and $–CH_3$ asymmetric bending mode of PLLA are at 1083, 1127, and 1450 cm^{-1} respectively. The FT-IR spectrums confirm that the MWCNTs have successfully functionalized and PLLA polymer chains has grafted from the sidewall of MWCNTs strongly.

The XPS analysis can be employed to determine the compositions on the surface of MWCNTs, the results are introduced in Figs. 5, 6, 7, and 8. Table 1 shows the XPS results of the functionalization of MWCNTs with the relative contents of

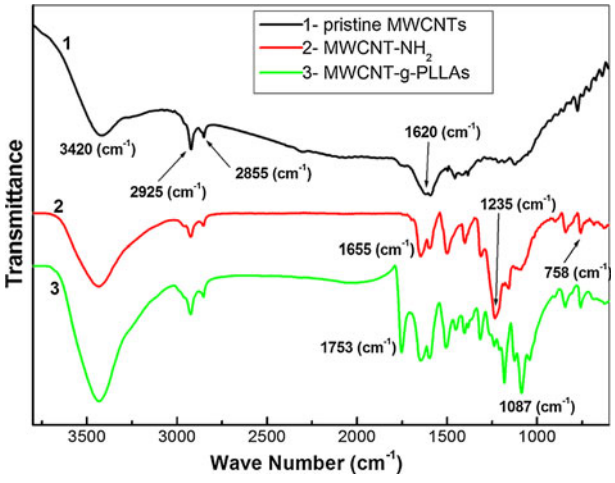

Fig. 4 FT-IR spectra of pMWCNTs (*1*), MWCNT–NH_2s (*2*), and MWCNT-*g*-PLLA (*3*)

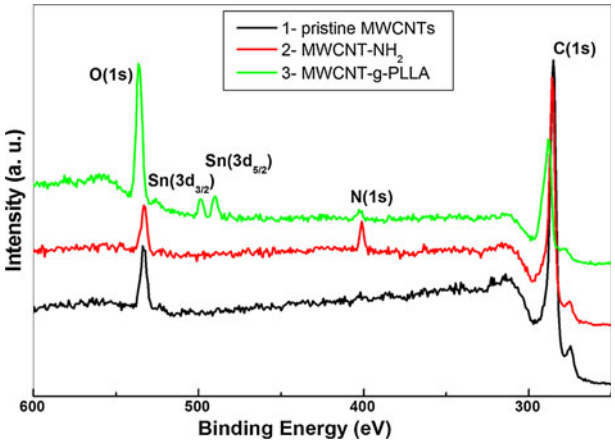

Fig. 5 The wide scan XPS spectra of pMWCNTs (*1*), MWCNT–NH_2s (*2*), and MWCNT-*g*-PLLAs (*3*)

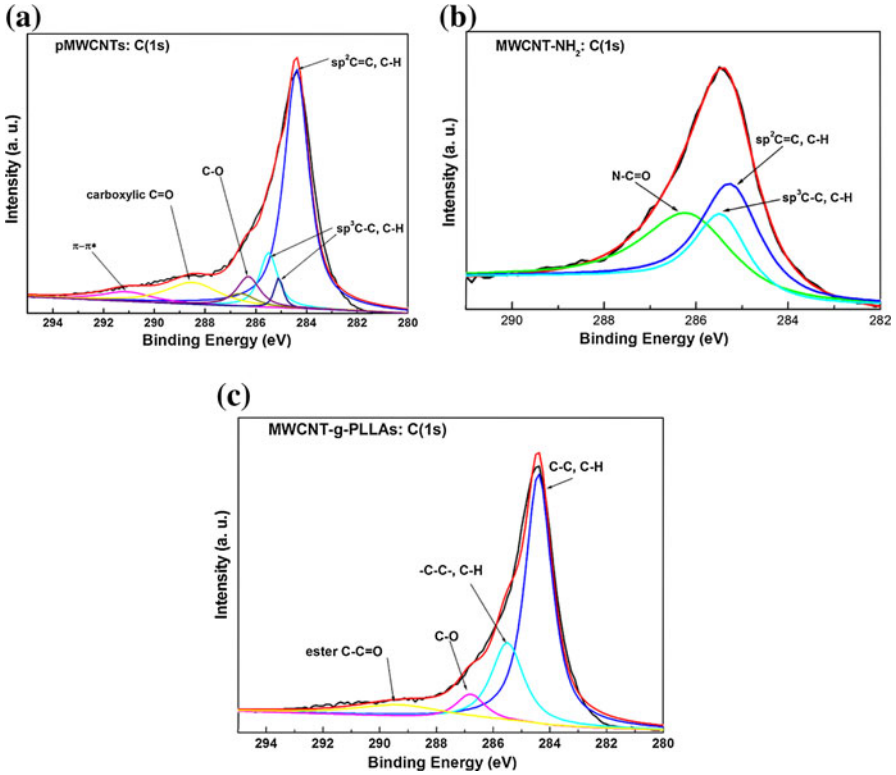

Fig. 6 The high-resolution XPS analysis at C(1*s*) region of pMWCNTs (**a**) MWCNT–NH_2s (**b**), and MWCNT-*g*-PLLAs (**c**). with data deconvolution of C(1*s*) region

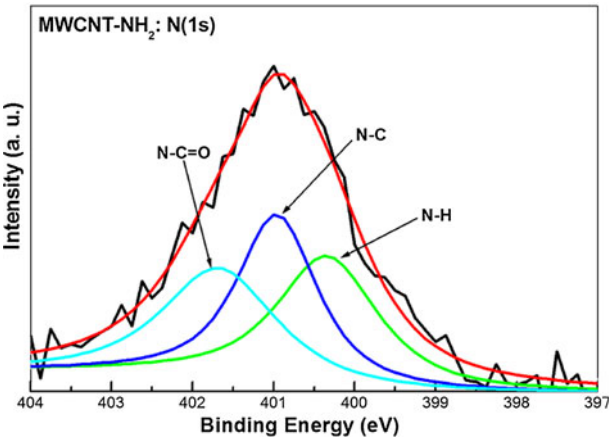

Fig. 7 The high-resolution XPS analysis at N(1*s*) region of MWCNT–NH_2s with data deconvolution of N(1*s*) region

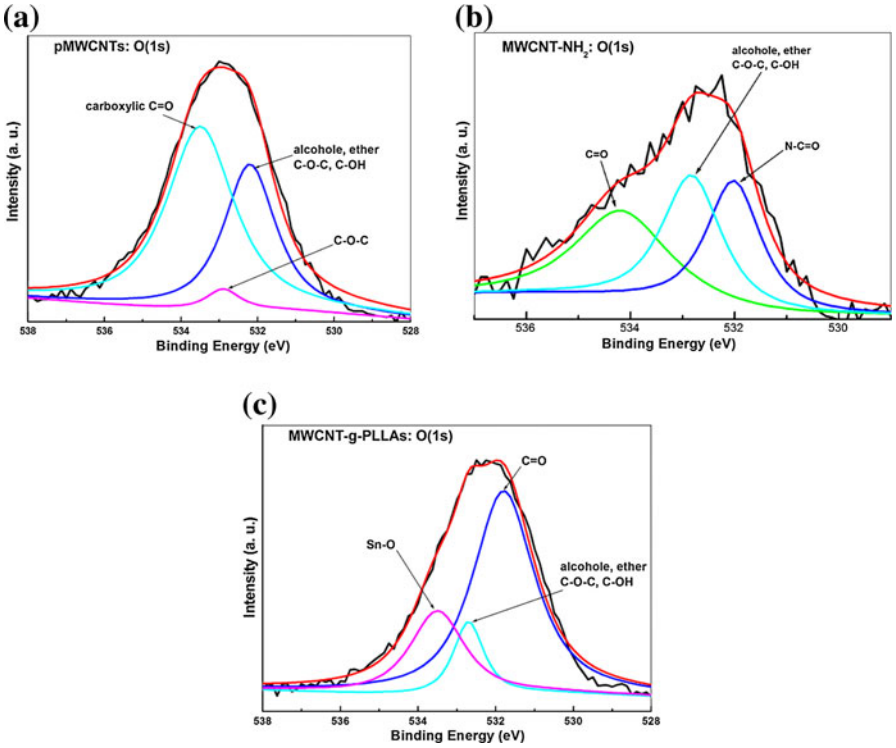

Fig. 8 The high-resolution XPS analysis at O(1*s*) region of pMWCNTs (**a**), MWCNT–NH_2s (**b**), and MWCNT-*g*-PLLAs (**c**). with data deconvolution of O(1*s*) region

Table 1 The XPS analysis of pristine and functionalized MWCNTs

Materials	Element	Peak (ev)	Atomic%
pMWCNTs	C(1*s*)	285.3	89.2
	O(1*s*)	533.9	10.8
MWCNT–NH_2s	C(1*s*)	287.3	85.6
	N(1*s*)	401.8	5.2
	O(1*s*)	534.5	9.2
MWCNT-*g*-PLLAs	C(1*s*)	285.3	66.0
	N(1*s*)		1.8
	O(1*s*)	532.7	31.5
	Sn($3d_5$)		0.6

carbon, nitrogen, and oxygen expressed as atomic percentage (atomic%), as a function of acylation and PLLA grafting.

The major peak component at the binding energy (BE) about 285 eV is assigned to the C(1*s*), the peak component at BE of 532 eV is attributed to O(1*s*) on the surface of MWCNTs, the peak at the BE of 401.8 eV corresponds to N (1*s*), the peak at the BE of 488 eV corresponds to Sn($3d_{5/2}$), and the peak at the BE of 496 eV corresponds to Sn($3d_{3/2}$) of the initiator groups on functionalized MWCNTs. The XPS analysis of pMWCNTs shows that the surface of pMWCNTs has some oxygen atoms that refer to the defects and impurities (C–H, C–O, C=O) that formed during manufacturing and storage before using. The peak, commonly related to the π–π* transition levels (free electrons of the graphitic plane) is observed at 291 eV.

After acylation of pMWCNTs, it can be seen that the amount of nitrogen atoms increased gradually that attributes to the amine groups. The XPS spectrum of acylated MWCNTs C(1*s*) peak shows a significant high intensity at a higher binding energy region. This peak is resulted from the amine groups on the tube surfaces. The existence of the O(1*s*) peak provides an additional evidence of MWCNT acylation. The presence of N–C and N–H bonds on the tube surfaces offers possibilities for tailoring MWCNT surface functionalization**.**

In case of grafting PLLA chains from the sidewall of MWCNT–NH_2s, increasing in concentration of O(1*s*) and detection of –C=O, O–H, and C–O bonds, indicates that PLLA chains grafted form the surface of MWCNTs successfully. Also, the disappearance of the π–π* transition levels indicates that covalent bonds should have been formed between the MWCNTs and PLLA in the time of grafting. These XPS spectra provide the evidence for functionalization of MWCNTs. The Sn–O bond refers to the initiator at the end of each grafted PLLA polymer chains that remained after polymerization [29–31].

Crystallinity of MWCNTs

The XRD patterns of pristine and functionalized MWCNTs are shown in Fig. 9. The pattern refers to pMWCNTs shows three peaks. The diffraction at 21° attributed to the impurities such as amorphous carbon. The peaks at 26.07°and 39.4°

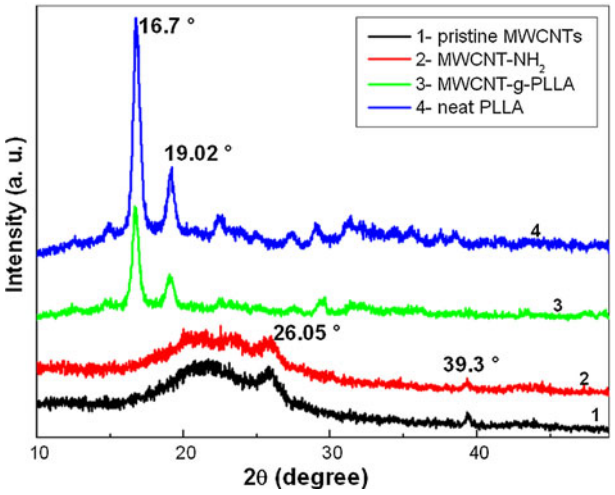

Fig. 9 The XRD patterns of pMWCNTs (**a**), MWCNT–NH_2s (**b**), and MWCNT-*g*-PLLAs (**c**)

corresponding to the (002, 3.47 Å) and (100, 2.12 Å) reflections of the carbon atoms, respectively, from the graphene plains that they refer to the walls of MWCNTs. The XRD patterns of MWCNT–NH_2 displayed the presence of two peaks at 26.07° and 42.7° (2.12 Å) corresponding to the (002) and (100) reflections from the graphene plains. It can be seen that the diffraction peaks of amorphous carbon are decreased because of purification during acylation. As can be seen in Fig. 9(3), the XRD pattern of MWCNT-*g*-PLLAs shows two significant diffraction peaks at 16.7° and 19.06° which characterize the crystallinity of PLLA-grafted polymer chains on the sidewall of MWCNTs. As can be seen, the peaks at 16.7° and 19.06° which characterize the crystalline phase of neat PLLA (Fig. 9(4)), reveal typical of α-form described as pseudo-orthorhombic, pseudo-hexagonal, or orthorhombic [35, 36]. It is found that not only the PLLA chains grafted on the sidewall of MWCNTs but also the grafted PLLA has the crystalline phase of the same as neat PLLA. Hence, the MWCNT-*g*-PLLA as heterogeneous nucleation points increase the crystallinity of composites.

Properties of composites

The molecular weight of prepared PLLA is characterized using GPC. It is found that the $\overline{Mw} = 272625$, $\overline{Mn} = 147641$, and P.I. = 1.84. It means that the prepared polymer has a good quality.

Figure 10 presents the stress versus strain curves of neat PLLA and its composites with various concentrations of MWCNT-*g*-PLLAs. The results show that the incorporation of MWCNT-*g*-PLLAs leads to the best overall reinforcing effect in modulus, yield stress, ultimate strength, and elongation. The tensile properties of neat PLLA and its composites are listed in Table 2. In order to

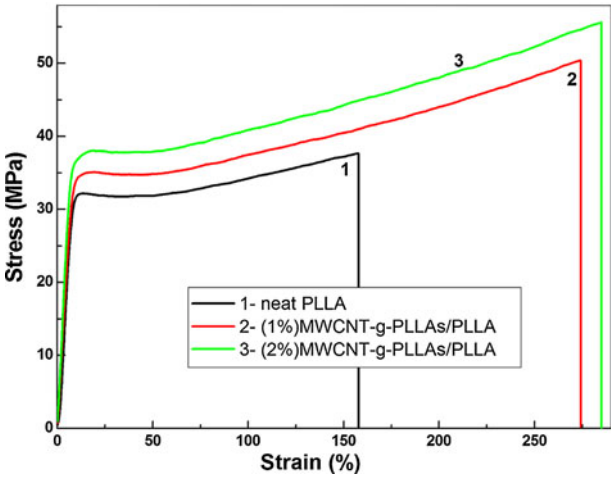

Fig. 10 The stress versus strain curves of neat PLLA and its composites with various concentrations of MWCNT-*g*-PLLAs

Table 2 Tensile test results of neat PLLA and it's composite with MWCNT-*g*-PLLAs

MWCNT-*g*-PLLAs (wt%)	Modulus (MPa)	Yield strength (MPa)	Ultimate strength (MPa)	Elongation (%)
0	4.1	32.3	37.8	158
1	4.5	35.2	50.4	274
2	5.1	38.3	55.8	285

understand the mechanisms of the tensile stress fracture of PLLA composites made from MWCNT-*g*-PLLAs, the SEM studies of ruptured areas of tensile test samples are carried out. Figure 11 gives the fracture cross-section of neat PLLA polymer and its composites that were created after tensile test. It can be seen that the fracture surface of neat PLLA is smooth. At the fracture surface of the (2 wt%)MWCNT-*g*-PLLAs/PLLA composite, it is shown that the MWCNT-*g*-PLLAs are not only well dispersed throughout the matrix but also their adhesion effect between MWCNTs and PLLA matrix is also greatly improved since most of the MWCNT-*g*-PLLAs on the fracture surface are pulled out. Therefore, the functionalization effectively improves the dispersion and interfacial bonding in MWCNTs-reinforced PLLA polymer composite.

The schematic representation of load transfer of tensile stress in composites is given in Scheme 2. It can be seen that the tensile loading in MWCNT-*g*-PLLAs/PLLA completely transferred to the filler materials, eventually leading to a full breakage of the MWCNT-*g*-PLLAs. It reveals that the adhesion between the matrix and the MWCNT-*g*-PLLA has been significantly enhanced via grafting of polymer from MWCNTs.

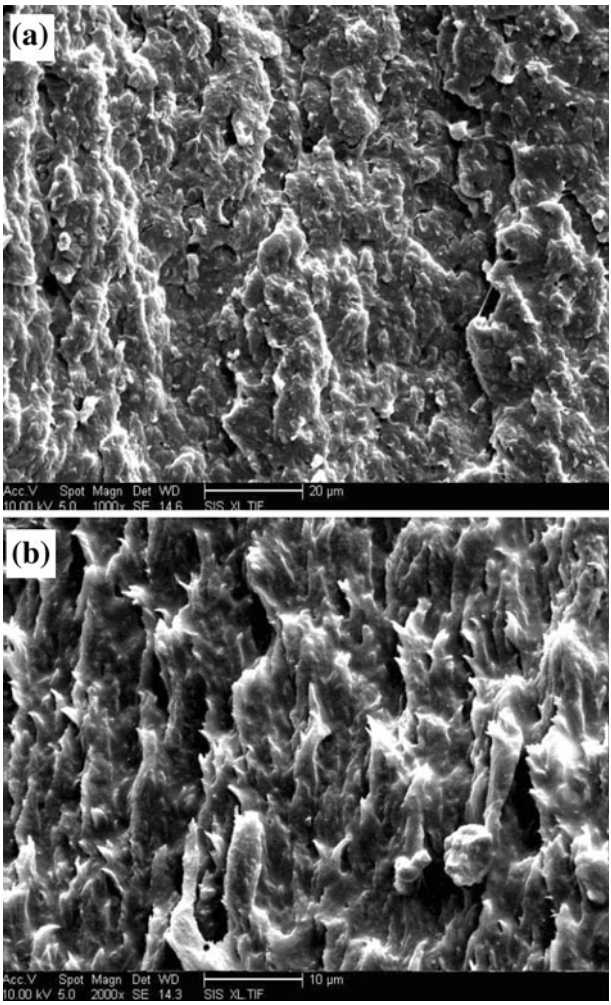

Fig. 11 The SEM micrographs of fracture surface refer to neat PLLA (**a**) and (2 wt%) MWCNTs-*g*-PLLA/PLLA composite (**b**)

PL analyze of neat PLLA, Fig. 12, shows a high intensity PL with a broad band at 505 nm. It can be seen that with increasing the concentration of MWCNT-*g*-PLLAs in composite, the PL increased. Also, two new wide peaks appeared at 395 and 443 nm, that refers to the effect of conjugation between MWCNT-*g*-PLLAs and neat PLLA as matrix. The peaks at 412 and 467 nm are the overlapping of 395 with 443 nm and the overlapping of 443 with 505 nm, respectively. The PL analysis of composites shows that the MWCNT-*g*-PLLAs enhanced the PL effect of PLLA. This characteristic helps the tracking of composite fragments at in vitro and in vivo researches of MWCNT-*g*-PLLAs/PLLA composites.

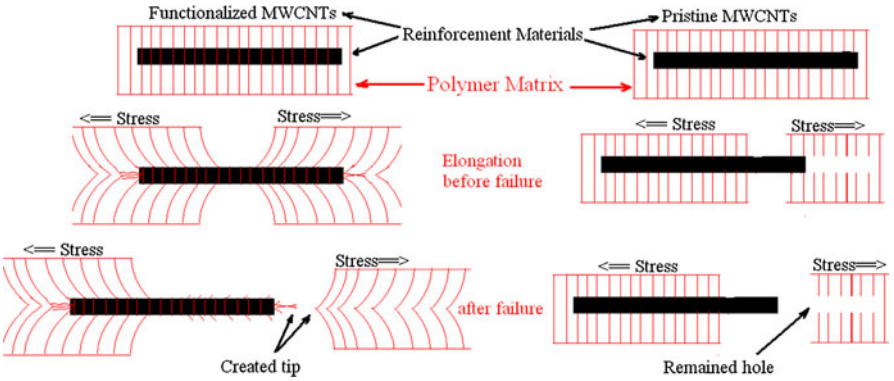

Scheme 2 Schematic representation of load transfer from matrix to filler in polymer composites reinforced with MWCNTs

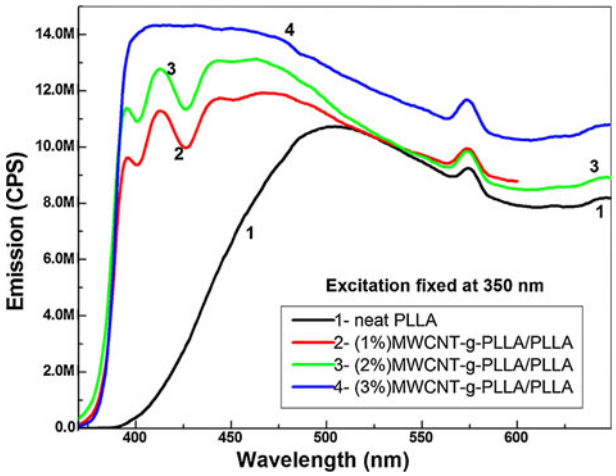

Fig. 12 The PL spectra of neat PLLA and its composites with various concentrations of MWCNT-*g*-PLLAs

Conclusions

An alternative grafting from approach based on in situ ring-opening polymerization of L-lactide oligomers is developed to covalently graft biodegradable PLLA polymer chains from the sidewall of pMWCNTs without shortening the MWCNTs. After grafting, core–shell structures with nanotubes as the hard shell and polymer layers as the soft shell are formed. Grafting of PLLA chains from the sidewall of MWCNTs would directly enhance the dispersion and compatibility of MWCNTs in PLLA as matrix. The incorporation of MWCNT-*g*-PLLAs leads to much better reinforcing and PL effect compared to pristine MWCNTs.

This research suggests that the properties of PLLA can be modified introducing a small percentage of functionalized MWCNTs. The combination of biodegradable polymers and CNTs opens in fact a new perspective in the self-assembly of nanomaterials and nanodevices for biomedical applications [37, 38].

Acknowledgment This study supported by the Excellent Youth Foundation of Heilongjiang Province of China (No. JC200715).

References

1. Ratna D, Karger-Kocsis JJ (2008) Recent advances in shape memory polymers and composites: a review. Mater Sci 43:254–269
2. Pohjonen T, Helevirta P, Tormälä P, Koskikare K, Patiälä H, Rokkanen P (1997) Strength retention of self-reinforced poly-L-lactide screws. A comparison of compression moulded and machine cut screws. J Mater Sci Mater Med 8:311–320
3. Loh XJ, Colin Sng KB, Li J (2008) Synthesis and water-swelling of thermo-responsive poly(ester urethane)s containing poly(epsilon-caprolactone). Biomaterials 29:3185–3194
4. Jeong SI, Kim BS, Kang SW, Kwon JH, Lee YM, Kim SH, Kim YH (2004) In vivo biocompatibilty and degradation behavior of elastic poly(L-lactide-co-e-caprolactone) scaffolds. Biomaterials 25:5939–5946
5. Lu XL, Cai W, Gao ZY, Tagn WJ (2007) Shape memory effects of poly(L-lactide) and its copolymer with poly(ε-caprolactone). Polym Bull 58:381–391
6. Freiberg S, Zhu X (2004) Polymer microspheres for controlled drug release. Int J Pharmaceutics 282:1–18
7. Welsher K, Liu Z, Sherlock SP, Robinson JT, Chen Z, Daranciang D, Dai H (2009) A route to brightly fluorescent carbon nanotubes for near-infrared imaging in mice. Nat Nanotechnol 4:773–780
8. Xua Z, Hub PA, Wanga S, Wang XB (2008) Biological functionalization and fluorescent imaging of carbon nanotubes. Appl Surface Sci 254:1915–1918
9. Iijima S (1991) Helical microtubules of graphitic carbon. Nature 354:56–58
10. Dai H (2002) Carbon nanotubes: Synthesis, integration, and properties. Acc Chem Res 35:1035–1044
11. Liu Z, Tabakman S, Welsher K, Dai HJ (2009) Carbon nanotubes in biology and medicine: in vitro and in vivo detection, imaging and drug delivery. Nano Res 2:85–120
12. Coleman JN, Khan U, Gunko YK (2006) Mechanical reinforcement of polymers using carbon nanotubes. Adv Mater 18:689–706
13. Moniruzzaman MI, Winey KI (2004) Polymer nanocomposites containing carbon nanotubes. Macromolecules 2006 39:5194–5205
14. Coleman JN, Cadek M, Blake R, Nikolosi V, Ryan KP, Belton C et al (2004) High-performance nanotube reinforced plastics: understanding the mechanism of strength increase. Adv Funct Mater 14:791–798
15. Mitchell CA, Krishnamoorti R (2007) Dispersion of single-walled carbon nanotubes in poly (e-caprolactone). Macromolecules 40:1538–1545
16. Sun L, Warren GL, O'Reilly JY, Everett WN, Lee SM, Davis D, Lagoudas D, Sue HJ (2008) Mechanical properties of surface-functionalized SWCNT/epoxy composites. Carbon 46:320–328
17. Zhang DH, Kandadai MA, Cech J, Roth S, Curran SA (2006) Poly(L-lactide) (PLLA)/multiwalled carbon nanotube (MWCNT) composite: characterization and biocompatibility evaluation. J Phys Chem B 110:12910–12915
18. Tsuji H, Kawashima Y, Takikawa H, Tanaka S (2007) Poly(L-lactide)/nano structured carbon composites: Conductivity, thermal properties, crystallization, and biodegradation. Polymer 48: 4213–4225
19. Daniel AU, Chang MKO, Andriano KP (1990) Mechanical properties of biodegradable polymers and composites proposed for internal fixation of bone. J Appl Biomater 1:57–78
20. Maquet V, Boccaccini AR, Pravata L, Notingher I, Jerômé R (2003) Preparation, characterization, and in vitro degradation of bioresorbable and bioactive composites based on bioglass-filled poly-lactide foams. Biomed Mater Res A 66:335–346

21. Bleach NC, Nazhat SN, Tanner KE, Kellomaki M, Tormala P (2002) Effect of filler content on mechanical and dynamic mechanical properties of particulate biphasic calcium phosphate–polylactide composites. Biomaterials 23:1579–1585
22. Kasuga T, Ota Y, Nogami M, Abe Y (2001) Preparation and mechanical properties of polylactic acid composites containing hydroxyapatite fibers. Biomaterials 22:19–23
23. Zhang D, Kandadai MA, Cech J, Roth S, Seamus A, Curran SA (2006) Poly(L-lactide) (PLLA)/multiwalled carbon nanotube (mwcnt) composite: characterization and biocompatibility evaluation. J Phys Chem B 110:12910–12915
24. Wu D, Wu L, Sun Y, Zhang M (2007) Rheological properties and crystallization behavior of multiwalled carbon nanotube/poly(ε-caprolactone) composites. J. Polym Sci B 45:3137–3147
25. Wu D, Zhang Y, Zhang M, Yu W (2009) Selective localization of multiwalled carbon nanotubes in poly(ε-caprolactone)/polylactide blend. Biomacromolecule 10:417–424
26. Jana RN, Cho JW (2008) Thermal stability, crystallization behavior, and phase morphology of poly(ε-caprolactone) diol-grafted-multiwalled carbon nanotubes. J Appl Polym Sci 110:1550–1558
27. Chen GX, Kim HS, Park BH, Yoon JS (2007) Synthesis of poly(L-lactide)-functionalized multiwalled carbon nanotubes by ring-opening polymerization. Macromol Chem Phys 208:389–398
28. Kim HS, Park BH, Yoon JS, Jin H (2007) Thermal and electrical properties of poly(L-lactide)-graft-multiwalled carbon nanotube composites. Eur Polym J 43:1729–1735
29. Saeed K, Park SY, Lee HJ, Baek JB, Huh WS (2006) Preparation of electrospun nanofibers of carbon nanotube/polycaprolactone nanocomposite. Polymer 47:8019–8025
30. Saeed K, Park SY (2007) Preparation and properties of multiwalled carbon nanotube/polycaprolactone nanocomposites. J Appl Polym Sci 104:1957–1963
31. Chen GX, Shimizu H (2008) Multiwalled carbon nanotubes grafted with polyhedral oligomeric silsesquioxane and its dispersion in poly(L-lactide) matrix. Polymer 49:943–951
32. Zeng HL, Gao C, Yan DY (2006) Poly(e-caprolactone)-functionalized carbon nanotubes and their biodegradation properties. Adv Funct Mater 16:812–818
33. Nabipour Chakoli A, Wan J, Feng JT, Amirian M, Sui JH, Cai W (2009) Functionalization of multiwalled carbon nanotubes for reinforcing of poly(L-lactide-co-ε-caprolactone) biodegradable copolymers. Appl Surface Sci 256:170–177
34. Yoon JT, Lee SC, Jeong YG (2010) Effects of grafted chain length on mechanical and electrical properties of nanocomposites containing polylactide-grafted carbon nanotubes. Compos Sci Technol 70:776–782
35. Miyata T, Masuko T (1997) Morphology of poly(L-lactide) solution-grown crystals. Polymer 38:4003–4009
36. Pirlot C, Willems I, Fonseca A, Nagy JB, Delhalle J (2002) Preparation and characterization of carbon nanotube/polyacrylonitrile composites. Adv Eng Mater 4:109–115
37. Wick P, Manser P, Limbach LK, Dettlaff-Weglikowska U, Krumeich F, Roth S, Stark WJ, Bruinink A (2007) The degree and kind of agglomeration affect carbon nanotube cytotoxicity. Toxicol Lett 168:121–131
38. Wei W, Sethuraman A, Jin C, Monteiro-Riviere NA, Narayan R (2007) Biological properties of carbon nanotubes. J Nanosci Nanotechnol 7:1–14